MAGNETIC ACTIVITY OF YOUNG LATE-TYPE STARS

K. N. Grankin [a*]

[a] *Crimean Astrophysical Observatory, 298409, Nauchny, Crimea, Russia*

Most young stars exhibit a large number of solar-like activity phenomena such as strong X-ray emission, flares, dark spots, wind, activity cycles, etc. Activity phenomena are believed to be a by-product of the nagnetic fields generated by young stars within their convective envelopes through dynamo processes. However, young stars show the existence of strong magnetic field (up to several kG), weak differential rotation, and the absence of a radiative core. All these facts challenge modern dynamo models. We review various manifestations of activity and some magnetic properties of young stars such as field strength, large-scale topology, differential rotation, and activity cycles. In particular, we point out such features of the young stars activity as the presence of vast spotted regions (up to 80% of the stellar surface), the long-term stability of the phase light curves, the absence of differential rotation (for some objects), the presence of axisymmetric and poloidal structures of the large-scale magnetic field, and some others. We then proceed to discuss the relationship between magnetic field topology, coronal X-ray emission, rotation, stellar age, and activity throughout the evolution of young stars and to compare these dependencies with the results for more evolved stars. Finally, we discuss our insight into the stellar magnetism origin and its impact on the early evolution of young convective stars.

Keywords: stars: activity – stars: magnetic fields – stars: evolution – stars: rotation

1. INTRODUCTION

Young late-type stars of about one solar mass at an age of a few million years are referred to as T Tauri stars (TTS). TTS appear at the stage of stellar evolution prior to the main sequence (PMS). These objects are divided into two subgroups - classical TTS (CTTS), which are still surrounded by protoplanetary gas-dust

* E-mail: konstantin.grankin@craocrimea.ru

disks, and TTS with weak emission lines (WTTS), which do not show any signs of disk accretion. Many WTTS exhibit a large number of solar-like activity phenomena such as strong X-ray emission, flares, dark spots, wind, activity cycles, etc. In other words, these stars are counterparts of the young Sun at an age of several million years.

The evolutionary status of TTS is clearly seen in the Hertzsprung-Russell (HR) diagram (see Fig. 1). These HR diagrams show 45 CTTS and 44 WTTS from the star-forming region of Taurus-Auriga (SFR Tau-Aur), which is about 140 pc away from us [1]. Most objects are located above the initial main sequence and are age of 1 to 10 million years. In the diagram, objects above the red line have no radiative core, i.e., following modern stellar evolution models, these are fully convective protostars.

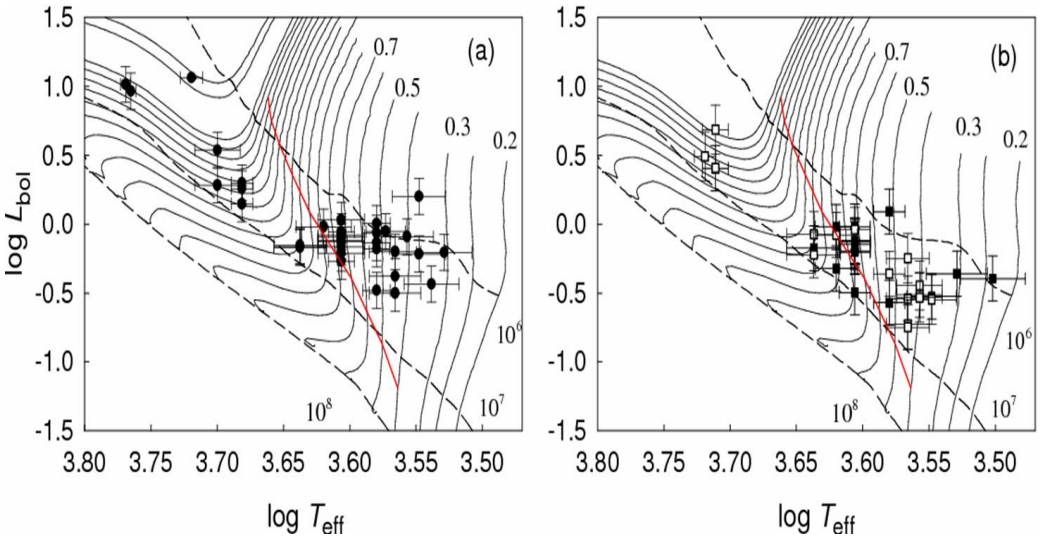

Fig. 1. HR diagram for CTTS (a) and WTTS (b) - from [1]. The solid lines mark the evolutionary tracks calculated with Y = 0.277 and Z=0.02 - for stars with different masses from 0.2 to 2.7 $M_\odot$. The dashed lines indicate isochrones for ages of 10^6, 10^7, and 10^8 yr. The author adopts a grid of evolutionary tracks from [2] computed for PMS stars. Objects above the red line have no radiative core.

The evolution features of TTS during the first million years are determined by the presence of strong magnetic fields (up to 4 kG) and the presence of circumstellar disks. On the one hand, magnetic fields and external deep convective shells of protostars are a reason for the existence of extended cold spots, hot facular fields, excessive chromospheric and coronal emission, short bursts, and other manifestations of solar-type activity observed among WTTS. On the other hand, magnetic fields play a key role in the complex processes of interaction between the central

star and the disk surrounding it. These processes lead to an angular momentum redistribution of the star-disk system and to the development of magnetospheric accretion processes, which are characteristic of CTTS and which are responsible for the formation of collimated jets, stellar and disk winds, and possibly for planet formation and migration.

2. EXTENDED COLD SPOTS

The existence of extended cold spots or spottedness areas is confirmed by the results of multicolor photometric observations, which made it possible to detect periodic brightness changes in most WTTS with amplitudes from $0.^m1$ to $0.^m6$ [3]. Changes in the amplitude of the periodic signal and the average brightness level from season to season have been recorded. The authors of this work showed that (1) the change in the amplitude of the periodic signal is also accompanied by a change in the shape of the phase light curve, and (2) the evolution of the amplitude and shape of the phase curve reflects changes in the area and distribution of spots.

Some of the youngest and most active WTTS have demonstrated the stability of the minimum brightness phase over many years. This phenomenon is most clearly observed for V410 Tau, whose minimum brightness phase has remained stable for at least 15–19 years (see Fig. 3 in [3]). This phenomenon is most likely due to the prolonged existence of the so-called active longitudes.

However, "there is nothing permanent under the Sun". The same V410 Tau showed a radical change in the photometric behavior in 2006-2009 [4]. The variability amplitude has gradually decreased from $0.^m6$ to $0.^m06$ for several seasons. At the same time, the average light level hasn't changed much. A simple modeling showed that this decrease in amplitude is accompanied by a decrease in the non-uniformity in spot distribution from 38 to 5-6%. Notably, the spots are almost evenly distributed over the surface when the light curve has a minimum amplitude. Previously, it was believed that the minimum amplitude is a sign of a decrease or disappearance of spots. These new conclusions were perfectly confirmed by the results of Doppler mapping - the latter showed that there are many spotted regions fairly evenly distributed along the equator (Fig. 4 in [5]).

Analysis of long-term multicolor photometric data using a simple two-component photometric model showed that the spotted areas are colder than the surrounding photosphere by 600-1500K and can cover from 30 to 90% of the stellar surface [6], [7]. These results were recently confirmed in a comprehensive study of the spectral and photometric data for the highly spotted star V1068 Tau [8]. Analysis of multicolor photometry together with optical and IR spectroscopy of high and medium spectral resolution showed that the spotted areas can cover

up to 80% of the visible surface of this star. Analysis of various photometric and spectroscopic data showed that many other low-mass stars with various evolutionary status also have large spots [3], [6], [7], [9], [10], [11], [12], [13].

3. CHROMOSPHERIC ACTIVITY AND FLARES

The lines H_α, H_β, HeI D3, IR triplet CaII and the doublet Ca II H & K are used as diagnostics of the chromospheric activity of young stars (see Fig. 4 in [14]). Equivalent widths of the residual emission in the cores of Hα, CaII H&K, and CaII IRT lines show clear modulations with the rotational phase and are ascribed to active chromospheric regions analogous to solar plages. The photospheric and chromospheric diagnostics do not correlate with each other [14]. A similar result was obtained for V410 Tau [15]. Particularly, the maximum contribution from the active chromospheric regions is observed very close to those times when the visible area of the photospheric spots is maximum.

The flare activity of TTS is not as high as that of flare red dwarfs. The most reliable information on the flare activity of TTS came from the analysis of continuous photometric observations within the space projects such as CoRoT, MOST, Kepler K2, and some others. Continuous MOST observations over 24 days made it possible to detect one flare in SU Aur [16] and TW Hya [17]. Kepler K2 monitoring, carried out for 80 days with a time resolution of about 30 minutes, recorded one flare in V1079 Tau [18].

Despite the clear superiority of space observations, ground-based photometry also provides important information on the flare activity of some selected TTS. In particular, simultaneous photometric monitoring from three different sites (Maidanak, Flagstaff and Sierra Nevada) made it possible to detect 9 flares in V410 Tau during November 2001 [19]. Observations were carried out during 11 nights with a time resolution of 4 to 20 minutes. The flare rate is about 2 events per day. Total energies involved in the events are $10^{35} - 10^{36}$ erg, except for the strongest one, which reaches 3×10^{37} erg. The authors showed that flares, typically, tend to occur mainly close to the minimum brightness of the star when its most active regions were turned to the observer. In addition to strong flare activity, a number of microflares were registered during the quiescent stages, as observed through the broad H_α component. If we compare flares in V410 Tau with flares in other active stars, then they surpass the strongest flares detected both in TTS and in other active stars like RS CVn type (see Fig. 10 in [20]).

4. SURFACE DIFFERENTIAL ROTATION

As a result of long-term spectropolarimetric studies of several most active WTTS, their surface differential rotation ($\Delta\Omega_{eq}$) was measured. The $\Delta\Omega_{eq}$ of

the 4 WTTS turned out to be much weaker than that of the Sun (see Table 1). The $\Delta\Omega_{eq}$ is small for V410 Tau [5], LkCa 4 [21], V819 Tau [22], and V830 Tau [22]. Only the $\Delta\Omega_{eq}$ for TAP 26 [23] is comparable to that for the Sun ($\Delta\Omega_{eq} = 0.0550\ rad\ d^{-1}$). But this star is noticeably older than other WTTS, its age is about 19 million years (My), while that of the remaining WTTS from this group is no more than 3 My.

Table 1. Differential rotation for some WTTS

Object	Ω_{eq} ($rad\ d^{-1}$)	$\Delta\Omega_{eq}$ ($rad\ d^{-1}$)	P_{rot} (day) equator – pole	P_{phot} (day), from [3]
V410 Tau	3.357 ± 0.0010	0.0070 ± 0.0060	1.872 – 1.876	1.871 – 1.877
LkCa 4	1.868 ± 0.0020	0.0100 ± 0.0060	3.364 – 3.382	3.367 – 3.387
V819 Tau	1.141 ± 0.0040	0.0080 ± 0.0080	5.510 – 5.550	5.50 – 5.61
V830 Tau	2.295 ± 0.0001	0.0156 ± 0.0009	2.719 – 2.756	2.738 – 2.747
TAP 26	8.819 ± 0.0003	0.0492 ± 0.0010	0.7124 – 0.7164	0.7135 – 0.7138

5. ANGULAR MOMENTUM EVOLUTION

Due to the effect of rotational modulation of cold/hot spots, the rotation periods of spotted TTS are known with high accuracy. For example, a sample of PMS stars with the known rotation periods in the direction of SFR Tau – Aur reaches 61 objects [24]. Analysis of the distribution of rotation periods for this sample of stars from SFR Tau-Aur showed that the rotation periods lie within a range from 0.5 to 10 days. In this case, 50 stars ($\sim 82\%$) exhibit rotation periods in the range from 0.5 to 4.5 days (fast rotators) and only 11 stars ($\sim 18\%$) have rather slow rotation with periods in the range from 5 to 10 days (slow rotators). A similar distribution of rotation periods is observed for other SFRs and young open clusters with an age of 1-5 My [25].

To date, rotation periods are known for hundreds of young stars in various regions of star formation and young open clusters. However, some unresolved problems remain. Firstly, these are the slow rotation rates of young stars. Secondly, it is unclear why the initial distribution of the angular momentum has a large dispersion. To explain the evolution of angular momentum during the first several million years, it is necessary to involve some process that would be responsible for the connection between the star and the disk. It has become apparent that rotational braking due to magnetized winds is strongly dependent on mass, and it is much less efficient at very low masses. Some form of decoupling between

the core and the envelope must be introduced in the model in order to simultaneously take into account the specific evolution of the spin of initially slow and fast rotators. All these issues are discussed in detail in [26].

6. AVERAGE MAGNETIC FIELD

Stellar magnetic fields are measured using the Zeeman effect, due to which some spectral lines expand under the influence of a magnetic field [27]. Thanks to the Zeeman-Doppler Imaging (ZDI) technique we can learn about topologies of the large-scale magnetic fields of TTS. This technique makes use of time-resolved spectropolarimetric observations of stars over several rotations to reconstruct distributions and orientations of the large-scale magnetic fields over their surfaces [28]. Analysis of the ZDI magnetic maps for several TTS showed the presence of strong and time-varying magnetic fields in the range from 100 to 1500 G [29]. In this case, the contribution of the dipole and octupole components varies widely.

It should be noted that the average magnetic fields of M-dwarfs, PMS stars, and brown dwarfs are comparable. This provides the natural conclusion that the origin of these magnetic fields can be of the same nature [30]. Analysis of an extended sample of PMS stars showed that the average large-scale magnetic field of young active stars decreases with increasing age, rotation period, and Rossby number [31]. It is noteworthy that TTS stars show a significant scatter in magnetic field values and lower Rossby numbers compared to M-dwarfs.

7. X-RAY EMISSION IN TTS

It is well known that there is a linear relationship between the X-ray luminosity and the total magnetic flux for various solar features (such as the quiet Sun, X-ray bright points, solar active regions, solar disk) and for late-type stars (dwarfs of spectral classes G, K and M) [32]. Young stars deviate somewhat from this linear dependence in the direction of lower X-ray luminosity. This relative deficit of X-ray luminosity may be due to the fact that stronger magnetic fields in TTS can suppress convective motions more efficiently (see Fig. 2 in [32]) .

According to the results of an X-ray survey of SFR Tau-Aur, the following interesting facts were revealed. Variations of UV emission may not have a strong correlation with the X-ray light curve (see Fig 8 in [33]). This means that accretion does not make a significant contribution to X-ray emission. Moreover, the origin of UV and X-ray emission may be different. Distinctions have been reported between the X-ray emission of accreting (CTTS) and non-accreting (WTTS) stars. Observations have suggested that accretion shocks could be responsible for part

of the X-ray emission from CTTS [34]. Some CTTS have a two-component X-ray spectrum, which consists of a little absorbed soft component and a strongly absorbed hard component. This little absorbed soft component can be generated at the base of the jets. The strongly absorbed hard component is time-varying and represents active coronal emission (see Fig. 5 in [35]).

The study of the relationship between the Rossby number and such magnetic activity parameters as the X-ray luminosity and magnetic flux density showed that saturation occurs at certain values of the Rossby number. Moreover, both active M-dwarfs and young open clusters stars and TTS are in saturation mode [30] and [36]. A recent generalized analysis of the rotation–activity relation for 821 solar-mass stars with different evolutionary status showed that the X-ray activity saturates when the ratio of L_X to L_{bol} reaches a level of about 10^{-3}. Outside the saturation mode, the X-ray luminosity depends only on the rotation period. In saturation mode, rotation dependence is also observed, but it is very weak (see Fig. 3 in [37]).

8. MAGNETIC FIELD TOPOLOGY

Zeeman-Doppler imaging (ZDI) is a tomographic method dedicated to the cartography of stellar magnetic fields, as well as surface brightness and temperature distributions. This method uses the ability of magnetic fields to polarize the emitted (or absorbed) light in spectral lines formed in a stellar atmosphere (Zeeman effect). Periodic modulation of Zeeman features during the rotation of a star is used to create an iterative reconstruction of the vector magnetic field on the stellar surface [38].

As a result of implementing three long-term international projects, MaPP [39], MaTYSSE [40] and TOUPIES [31], a lot of spectropolarimetric data were obtained for several tens of TTS using three spectropolarimeters (ESPaDOnS, NARVAL and HARPS) mounted on three telescopes: 3.6 m CHFT (Hawaii), 2 m TBL (Pic du Midi, France), and 3.6 m ESO (La Silla, Chile). Analysis of the spectropolarimetric data obtained within these three projects made it possible to reconstruct the large-scale structure of the magnetic field in both CTTS and WTTS (see [21], [23], [41]).

The first conclusions drawn from the features of the magnetic field topology of the accreting PMS stars were as follows [42]. (1) The contribution of the octupole component of the magnetic field relative to the dipole component increases with age. (2) Fully convective stars host predominantly simple axisymmetric fields and can have strong (∼kG) dipole components. (3) Stars with small radiative cores exhibit dominantly octupolar magnetic fields with weak dipole components that vary from 0.1 kG to of an order of ∼kG.

Based on these results, the stars with different internal structures were suggested to have different large-scale magnetic field topologies (see Fig. 2). Stars in region 1 have a developed radiative core and complex non-axisymmetric magnetic fields. Stars in region 2 have a small radiative core ($0 < M_{core}/M_* < 0.4$) and axisymmetric magnetic fields, in which, the octupole component largely dominates. Stars from region 3 are fully convective and show the axisymmetric field, in which a strong dipole component dominates. The fourth magnetic topology region exists at the lowest masses.

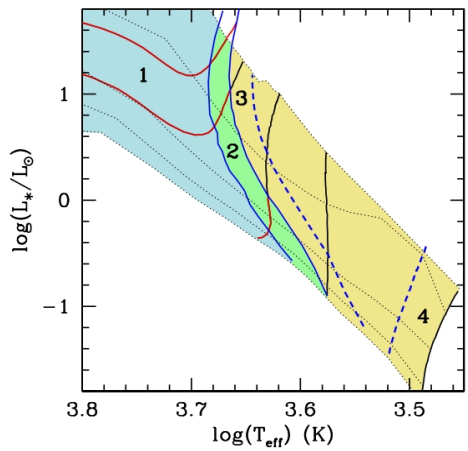

Fig. 2. H-R diagram - from [43]. PMS stars in the different numbered regions have differing internal structures and are observed to have different large-scale magnetic field topologies (see text for details).

If we compare the magnetic field topology of young stars with that of older stars with an age of more than 10 My, then we can draw the following preliminary conclusions. (1) TTS show stronger, more poloidal, and more axisymmetric magnetic fields than older objects. (2) The diagram of the Rossby number dependence on age shows that the magnetic dynamo of young stars is significantly different than that in older stars with radiative cores. (see Fig. 10 from [31]).

9. MAGNETIC FIELDS AND STAR-DISC INTERACTIONS

Even within the TTS subgroup, the magnetic field topology can vary greatly. Stars with simple large-scale (predominantly dipole) magnetic field configurations (as in the case of AA Tau) have stronger fields, are slower rotators, and exhibit larger X-ray emitting coronae than stars with more complex and weaker magnetic fields (as in V2247 Oph). Based on this we can conclude that the field complexity controls the distribution of open and closed field regions across the stellar surface,

and strongly influences the location and shapes of accretion hot spots (see Fig. 1 in [29]).

More specifically, a predominantly dipolar and stronger field of AA Tau causes accretion footpoints to be located at higher latitudes ($< B >= 1220\ G$, $B_{dip} = 1720\ G$, $B_{oct} = 500\ G$). The material accreting onto TW Hya is deflected towards the mid-latitudes due to its sufficiently strong octupole field component ($< B >= 1610\ G$, $B_{dip} = 730\ G$, $B_{oct} = 3100\ G$). The more complex and weaker field of V2247 Oph ($< B >= 220\ G$, $B_{dip} = 110\ G$, $B_{oct} = 230\ G$) leads to a complex accretion pattern at mid and low latitudes (see Fig. 3).

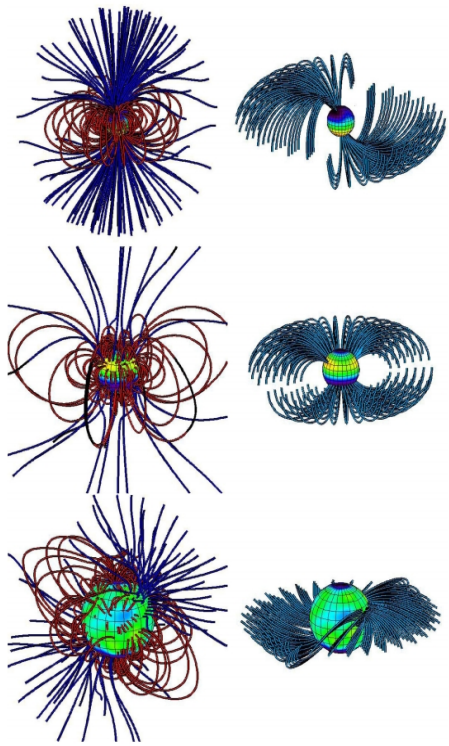

Fig. 3. Potential field extrapolations for AA Tau (upper panels), the TW Hya 2010 field (middle panels) and V2247 Oph (lower panels) showing closed and open field lines (left-hand panels) and accreting field lines (right-hand panels) - from [29] (see text for details).

Simulations of the magnetic field interaction with the disk internal parts showed that as the strength of the dipole component decreases, and the complexity of the field structure increases, the outer edge of the closed corona, the inner edge of the disk, and the region in which the star's magnetic field can disrupt the disk, they all move closer to the star (see Fig. 4). If CTTS have solar-like

magnetic cycles, then we would expect the cycles to exist in the position of the inner edge of the accretion disk and the location of accretion footpoints.

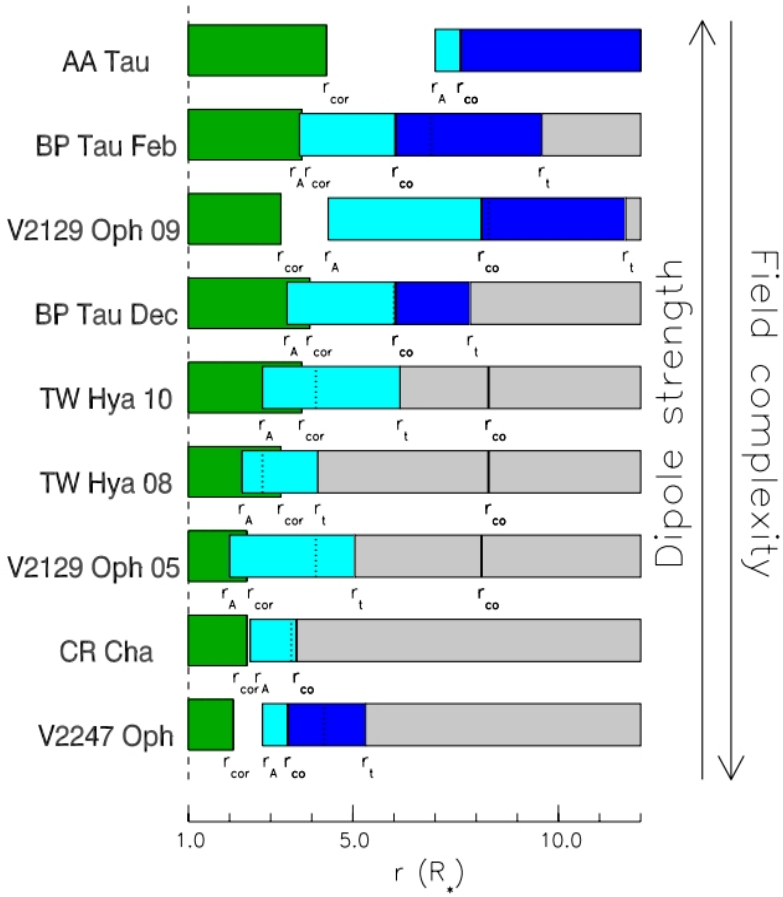

Fig. 4. Coronal extents (r_{cor}), Alfvén surface radii (r_A) and torque balance radii (r_t) depending on the strength of the dipole component of the field and the field complexity, from [29]. The horizontal direction is measured in stellar radii from the stellar surface. The extent of the closed corona is shown in green. The light blue bar shows the range of radii from which accretion can occur onto the star. The dark blue bar shows the range of radii where the magnetic field can disrupt the disc outside the corotation radius (r_{co}). As the dipole components weaken, the outer edge of the corona and the inner edge of the disc moves inwards.

10. ACTIVITY CYCLES AND MAGNETIC FIELD TOPOLOGY

The most reliable sign of the existence of a stellar activity cycle is the detection of periodic changes in the disk integrated emission in calcium lines. Unfortunately,

there are no such multi-decade chromospheric observations for PMS stars. However, such observations were made for the more evolved solar-like stars at the Mount Wilson Observatory (for example, [44], [45]).

There are now numerous stars that have been characterised by the ZDI mapping and also have a chromospherically determined cycle period in the literature. It is obvious that even a single ZDI map for one chromosphere-active star contains useful information on the magnetic field topology - such as how much magnetic energy is stored in toroidal or axisymmetric modes. An interesting analysis of the magnetic properties of a sample of stars that have at least one ZDI map as well as a chromospheric activity cycle period has recently been made [46].

Two groups of stars in the cycle period versus the rotation period diagram were identified. One group of stars belongs to the so-called inactive branch, another group lies on the active branch. The authors find some evidence that stars along the active branch show significant average toroidal fields that exhibit large temporal variations while stars exclusively on the inactive branch have dominantly poloidal fields throughout their entire cycle (see Fig. 5). The reason for this behaviour may be due to different dynamo modes operating along the active and inactive branches as proposed in [47].

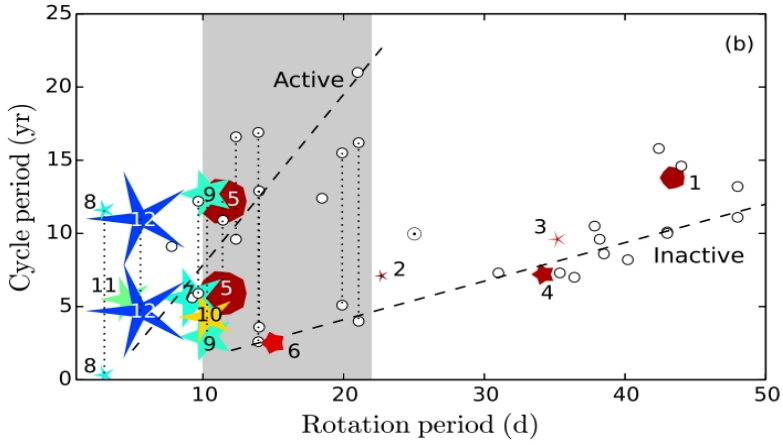

Fig. 5. Chromospheric activity cycle period against rotation period, from [46]. The symbol colour represents the poloidal energy fraction (ranging from red for purely poloidal to blue for purely toroidal) and symbol shape represents how axisymmetric the poloidal component of the field is (ranging from decagons for a purely axisymmetric poloidal field to pointed stars for a purely non-axisymmetric field). Dashed lines indicate the active and inactive branches. Stars with multiple cycle periods are connected with a dashed line. The shaded region indicates the range of rotation periods where the active and inactive branches overlap.

11. PROPERTIES OF THE YOUNG STARS

All TTS rotate faster than the Sun ($P_{rot} \sim 1 - 10$ days). Many TTS are in saturation when the magnetic field and X-ray luminosity are weakly dependent on the rotation period (Rossby number). Some of the youngest TTS have very strong large-scale magnetic fields (up to 3-4 kG) with a predominance of the dipole component. Such objects have extended (up to 80% of the visible stellar surface) long-lived (up to 15 years) spotted areas and exhibit very weak differential rotation. It is clear that during the PMS sequence phase young stars go through important structural and global changes. Aside from the appearance of a radiative core in solar-like stars by the time they reach the ZAMS, these stars undergo a complex rotational history (see Sect. 5). Besides this, young stars for some period of their infancy are fully convective. It should be noted that M-dwarfs of late spectral classes (M5-M9) exhibit very similar properties.

What impact does the high rotation rate have on turbulent convection, mean flows, and dynamo action in such stars?

Several groups have studied this topic with high performance numerical simulations. These simulations share common features with those of more evolved solar-like stars and low-mass stars (see a detailed review in [48]). We mention only some important and interesting modeling results here.

For fully convective low-mass stars, stratified convection models predict antisolar differential rotation, with the equator rotating slower than the poles. In this case, the equilibrated field strength of the dynamo was of order equipartition with flows near the surface [49].

Recent simulations have shown that despite a lack of the tachocline region, low-mass fully convective stars are capable of generating strong magnetic fields, indicating that a dynamo mechanism fundamentally different from the solar dynamo is at work in these objects [50]. A distributed dynamo working in the self-consistent 3D model spontaneously produces a dipole-dominated surface magnetic field of the observed strength. The interaction of this field with the turbulent convection in outer layers shreds it, producing small-scale fields that carry most of the magnetic flux. The authors made use of the ZDI technique to analyze the large-scale magnetic field of their simulation and recovered a strong polar spot of the radial field corresponding to the visible magnetic pole of the dipolar component present in their numerical simulation. The recovered magnetic field maps feature almost no toroidal component (less than 2% of the reconstructed magnetic energy) and are mostly axisymmetric.

The "thin flux tube" simulations of fully convective stars showed that in the absence of strong interior differential rotation, magnetic fields tend to emerge near the stellar poles [51]. Thus, the polar spots inferred at the surface of M-dwarfs

might conceivably arise either from global-scale dipole fields that locally diminish convective heat transport (as in [50]), or from a collection of smaller-scale flux tubes that are built in the interior and emerge (as in [51]), or a combination of both.

Interesting conclusions regarding the evolution of stellar dynamo, magnetic field topology, and activity level in the PMS phase were obtained as a result of a series of 3D MHD simulations of stellar convective dynamo with the ASH code [52]. The authors selected five different models characterized by different radii of their radiative zone (0, 20, 40, 60, and 70% of the stellar radius), following an evolutionary track calculated from the 1D stellar evolution code. These models characterized stellar evolution from 1 to 50 My. By introducing a seed magnetic field in the fully convective model and spreading its evolved state through all four remaining cases, they register systematic variations in the dynamical properties and magnetic field amplitude, and topology of these models. The authors find that the magnetic field amplitude increases as it evolves towards the ZAMS. Moreover, the magnetic field topology becomes more complex when the axisymmetric component decreases and the non-axisymmetric one becomes predominant. The dipolar components decrease as the rotation rate and the size of the radiative core increase. The magnetic fields possess a mixed poloidal-toroidal topology with no obvious dominant component.

It should be noted that the generation of the mean magnetic field shows that as the convective zone becomes shallower and the rotation rate increases, the Ω effect becomes predominant in the generation of the mean toroidal magnetic field. Moreover, the α-effect tends to generate more poloidal field than the toroidal one. In other words, the authors of this work see a manifestation of the $\alpha - \Omega$ dynamo in each model. Three out of five MHD simulations display a magnetic cycle. In all cyclic cases, the time-latitude diagram of the longitudinally averaged toroidal magnetic field shows a clear poleward branch starting from low latitude (see Fig. 20 in [52]). The authors note that this magnetic field propagation is also compatible with the $\alpha - \Omega$ dynamo concept, as it satisfies the Parker-Yoshimura rule (see Fig. 22 in [52]).

MHD simulations have been performed to study the generation and evolution of a magnetic field in models that mimic young stars at two stages of evolution [53]. The first stage is at 1.1 My when the star is completely convective. The second stage is at 14 My when the star is partly convective with a radiative core developed up to 30% of the stellar radius. Analysis has shown that the star rotates almost rigidly at the fully convective phase, whereas at the partially convective phase there is a differential rotation with conical contours of iso-rotation. This agrees very well with observational results given in Sec. 4. Wherein, the magnetic field topology is different for these two models.

REFERENCES

1. Grankin K. N., AstL, 2016, **42**, 314
2. Siess L. et al., A&A, 2000, **358**, 593S
3. Grankin K. N. et al., A&A, 2008, **479**, 827
4. Grankin K. N. & Artemenko S.A., IBVS, 2009, **5927**, 1
5. Skelly M.B. et al., MNRAS, 2010, **403**, 159
6. Grankin K.N., AstL, 1998, **24**, 497
7. Grankin K.N., AstL, 1999, **25**, 526
8. Gully-Santiago M.A. et al., ApJ, 2017, **836**, 200
9. Chugainov P.F., IzKry, 1976, **54**, 89
10. Herbst W., 1989, AJ, **98**, 2268
11. Petrov P. P. et al., A&A, 1994, **107**, 9
12. Venuti L. et al., A&A, 2015, **581**, A66
13. Fang X.-S. et al., MNRAS, 2016, **463**, 2494F
14. Frasca A. et al., A&A, 2010, **518**, A48
15. Mekkaden M.V. et al. BASI, 2005, **33**, 433M
16. Cody A.M. et al., AJ, 2013, **145**, 79C
17. Siwak M. et al., SBCS Conf, 2017, 214
18. Alencar S.H.P. et al., A&A, 2018, **620**, 195A
19. Stelzer B. et al., A&A, 2003, **411**, 517
20. Fernandez M., et al., A&A, 2004, **427**, 263
21. Donati J.-F. et al., MNRAS, 2015, **453**, 3706
22. Donati J.-F. et al., MNRAS, 2014, **444**, 322
23. Yu L. et al., MNRAS, 2017, **467**, 1342
24. Grankin K.N., AstL, 2013a, **39**, 251
25. Bouvier J., et al., Conf. Protostars and Planets VI, 2014, pp 433–450
26. Gallet F. & Bouvier J., A&A, 2013, **556**, A36

27. Johns-Krull C. M. & Valenti J. A., ASPC, 2000, **198**, 371

28. Semel M., A&A, 1989, **225**, 456

29. Johnstone C. P. et al., MNRAS, 2014, **437**, 3202J

30. Reiners A., LRSP, 2012, **9**, 1R

31. Folsom C.P. et al., MNRAS, 2018, **474**, 4956F

32. Johns–Krull C.M., ASPC, 2009, **405**, 485

33. Audard M. et al., A&A, 2007, **468**, 379

34. Telleschi A. et al., A&A, 2007, **468**, 443

35. Gudel M., AN, 2008, **329**, 218

36. Grankin K.N., AstL, 2013b, **39**, 446

37. Reiners A. et al., ApJ, 2014, **794**, 144

38. Donati J.-F. & Brown S. F., A&A, 1997, **326**, 1135

39. Donati J.-F., et al., MNRAS, 2008, **386**, 1234

40. Donati J.-F., et al., MNRAS, 2014, **444**, 3220

41. Donati J.-F. et al., MNRAS, 2011, **412**, 2454

42. Gregory S.G. et al., IAUS, 2014, **302**, 40G

43. Gregory S.G. et al., ApJ, 2012, **755**, 97

44. Wilson O. C., ApJ, 1978, **226**, 379W

45. Baliunas S. L. et al., ApJ, 1995, **438**, 269B

46. See V. et al., 2016, MNRAS, **462**, 4442

47. Bohm-Vitense E., ApJ, 2007, **657**, 486B

48. Brun A.S. & Browning M.K., LRSP, 2017, **14**, 4B

49. Dobler W. et al., ApJ, 2006, **638**, 336D

50. Yadav R.K. et al., ApJL, 2015, **813**, L31

51. Weber M.A. & Browning M.K., ApJ, 2016, **827**, 95

52. Emeriau-Viard C. & Brun A.S., ApJ, 2017, **846**, 8

53. Zaire B. et al., IAUS, 2017, **328**, 30Z